Thin Solid Films xxx (2016) xxx–xxx

Contents lists available at ScienceDirect

Thin Solid Films

journal homepage: www.elsevier.com/locate/tsf

Post-deposition treatment of $Cu_2ZnSnSe_4$ with alkalis☆

G. Rey[a,*], F. Babbe[a], T.P. Weiss[a], H. Elanzeery[a], M. Melchiorre[a], N. Valle[b], B. El Adib[b], S. Siebentritt[a]

[a] Laboratory for Photovoltaics (LPV), Physics and Materials Science Research Unit, 41 rue du Brill, Belvaux L-4422, Luxembourg
[b] Luxembourg Institute of Science and Technology (LIST), 41 rue du Brill, Belvaux L-4422, Luxembourg

ARTICLE INFO

Article history:
Received 11 May 2016
Received in revised form 11 November 2016
Accepted 11 November 2016
Available online xxxx

Keywords:
Kesterite
Copper zinc tin selenide
Sodium
Potassium
Post-deposition treatment

ABSTRACT

Low temperature post-deposition treatment of $Cu_2ZnSnSe_4$ with NaF and KF significantly improved the solar cell efficiency (from 6.4% to 7.8% and 7.7% on average, respectively) due to enhanced fill factor (from 0.58 to 0.61 and 0.62), open-circuit voltage (V_{oc}) (from 314 mV to 337 mV and 325 mV) and short-circuit current density (from 35.3 mA • cm^{-2} to 38.3 mA • cm^{-2} and 38.6 mA • cm^{-2}). V_{oc} improvement was higher for solar cells with NaF treatment due to an increase in radiative efficiency at room temperature and shallower defect activation energy as determined by photoluminescence (PL) and temperature dependent admittance spectroscopy, respectively. In the case of KF treatment, red-shift of the PL, higher band tail density of state and donor activation energy deeper in the band gap were limiting further improvement of the V_{oc} compared to NaF treatment.

1. Introduction

Selenide kesterite semiconductor $Cu_2ZnSnSe_4$ (CZTSe), sulfide (CZTS) and sulfo-selenide (CZTSSe) counterparts have been considered as potential absorber materials in thin film solar cell [1] owing to their high absorption of solar light [2], to the tunable band-gap energy E_g falling in the optimal range for solar energy conversion [3] and due to the relatively high abundance of Cu, Zn and Sn compared to In and Te used in other thin film photovoltaic technologies such as $Cu(In,Ga)Se_2$ and CdTe. Like in $Cu(In,Ga)Se_2$, a closely related material, the inclusion of alkaline metals in kesterite induces profound modification of its morphological and electro-optical properties. The most efficient CZTSe device was produced using additional supply of Na [4].

When supplied during the formation of the kesterite thin film, Na enhances crystallite size [5], grain size [6–12] and improves film or surface morphology [7,8,11]. In both CZTSe and CZTS, atom probe tomography revealed that Na tends to segregate at the grains boundaries [13,14]. Na increases minority carrier lifetime in both single crystals [15] and polycrystalline thin films [16]. Non-radiative recombinations can be decreased by Na addition leading to higher photoluminescence (PL) yield [5,9]. The main effects of Na incorporation on the electrical properties are as follows: a decrease in acceptor activation energy [16–18], an increase in hole mobility [16,17,19] and an increase in carrier concentration [16,17], although this last point is not always observed for polycrystalline thin films [19]. The presence of Na at the kesterite surface depends strongly on the growth process [9,20] and an accurate control of Na concentration at the CdS/kesterite interface is necessary to achieve working solar cells [21]. Intentional doping of CZTS with K is reported to decrease the open-circuit voltage (V_{oc}) but to increase the external quantum efficiency (*EQE*) and thus the short-circuit current density (J_{sc}) [22].

From a theoretical point of view Na_{Cu}, Na_{Zn} and K_{Cu} are the most favourable substitutional defects [23–25] which are expected not to form deep-defects and should thus be benign for device efficiency. The interstitial incorporation of Na in the kesterite lattice is also likely due to its low formation energy [23]. The possibly detrimental substitutional deep-defects are Sn related and show a high formation energy [24].

The two main strategies to incorporate alkaline elements in kesterite is either to supply them during kesterite synthesis [5-7,11,12,16,19,22] or after the growth as a post-deposition treatment (PDT) [11,18]. Here we investigated PDT of CZTSe thin films using NaF and KF at low temperature (100 °C).

2. Experimental details

2.1. CZTSe growth and post-deposition treatment

CZTSe thin films were grown on a Mo-coated soda lime glass (SLG) substrate heated at 470 °C in a molecular beam epitaxy system

☆ Key: P87PX.
* Corresponding author.
E-mail address: germain.rey@uni.lu (G. Rey).

http://dx.doi.org/10.1016/j.tsf.2016.11.021

by co-evaporation of Cu, Zn, Sn, SnSe and Se. More details about the process can be found in Refs. [26,27].

An optional two step PDT was applied to the CZTSe thin films. The first step consisted of an approximately 5 nm thick alkaline fluoride layer deposition by electron beam evaporation. The second step was an annealing in a tube furnace at atmospheric pressure and 100 °C for 1 h under a N_2 atmosphere. Prior to solar cell processing, the samples, which underwent a PDT, were washed with deionized water.

2.2. Solar cell preparation

After a surface etching of the CZTSe thin films using KCN solution, solar cells were prepared by chemical bath deposition of a 50 nm thick CdS buffer layer [28]; followed by the deposition of an intrinsic ZnO layer (80 nm thickness) and a transparent conductive ZnO layer (380 nm thickness) by non-reactive magnetron sputtering [29]. Metallic contacts were achieved by a Ni/Al grid. 6 to 8 solar cells of about 10 × 5 mm^2 were tested for each preparation route.

2.3. Characterization

The global composition of the CZTSe films was measured by Energy dispersive X-ray spectroscopy using an accelerating voltage of 20 kV. Secondary ion mass spectrometry(SIMS) depth profiling was used to characterize the solar cells. The samples were bombarded by a 1 keV Cs+ beam. With these conditions, the elements of interest were detected as MCs+ clusters (M = Na, K, Zn, O, Cd, S, Se, Cu, Zn, Sn, Mo and F) to allow a quantitative comparison of Na and K contents between samples. A cold mirror halogen lamp calibrated with a silicon reference solar cell was used to illuminate the cells during current-voltage characteristic measurements (JV) and temperature dependent JV (JVT). Admittance spectroscopy (AS) recorded without bias voltage and capacitance-voltage measurements (CV) were performed with a precision LCR meter using 30 mV modulation amplitude. The solar cells were placed in a closed cycle He cryostat for temperature dependent measurements (JVT, AS or CV). For CV measurements, the temperature (100–130 K) and the frequency (1 kHz) were set according to Ref. [30]. The *EQE* was measured using lock-in technique using a monochromated light source calibrated with Si and InGaAs photodiodes. The internal quantum efficiency (*IQE*) was derived from *EQE* by correcting for the absorptance of the CdS and ZnO front layers and for the device reflectance [31], both measured with an UV-vis-NIR spectrophotometer. The PL was measured at room temperature with an InGaAs detector under a continuous red excitation of 6.6 $kW \cdot m^{-2}$.

3. Results and discussion

Untreated absorbers, absorbers treated with NaF and absorbers treated with KF were investigated. Those sets will hereafter be referred to as “Std”, “NaF” and “KF” respectively. The absorber film composition prior to any PDT was Cu-poor $\frac{Cu}{Zn+Sn} = 0.8$ and Zn-rich $\frac{Zn}{Sn} = 1.27$ which is the composition leading to the most efficient CZTSe based solar cell [4,8].

The SIMS profiles of Na and K are shown in Fig. 1 where the solar cells were sputtered from the top (ZnO, CdS) to the SLG substrate. NaF-PDT did not significantly change the Na incorporation into the film which is mainly controlled by Na diffusion from the SLG. Nonetheless Na-PDT could possibly change the Na concentration at the very top of the CZTSe surface and at the grain boundaries without changing the SIMS profile because of the large amount of Na already present in the film. KF-PDT was found to effectively increase K concentration throughout the CZTSe film.

The JV parameters of the solar cells are plotted in Fig. 2. PDT with NaF and KF increased the average conversion efficiency *eff* from 6.4% to 7.8% and 7.7%, respectively. It is interesting to notice that the PDT without supply of alkaline fluoride (AW) has a detrimental effect on the *eff*, therefore the improvement seen with NaF-PDT or KF-PDT can be attributed unambiguously to the presence of alkaline fluoride. For both NaF-PDT and KF-PDT the improved *eff* is resulting from an increase in all solar cell parameters such as fill factor *ff*, V_{oc} and J_{sc}. The *ff* rise under Na doping has been attributed to the increase of kesterite conductivity [16]. The J_{sc} enhancement is due to better collection of carriers generated by long-wavelength light, as seen in *EQE* (not shown) which can partly be attributed to a change in the space charge region width (derived from not shown CV) from 145 nm to 206 nm and 213 nm respectively for Std, NaF and KF. The PDT effect on J_{sc} is more pronounced for KF, in agreement with the significant increase in J_{sc} reported after K doping of CZTS [22]. The V_{oc} improvement by both PDT goes together with a drop of the reverse saturation current density, in average $J_0 = 1.05 \times 10^{-5}$, 3.7×10^{-6}

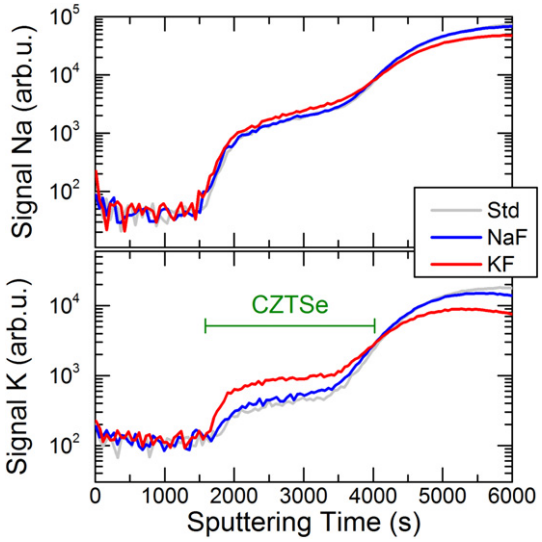

Fig. 1. SIMS profile of Na (top) and K (bottom) measured on solar cells based on CZTSe without PDT (Std), CZTSe with NaF or KF PDT (NaF, KF respectively).

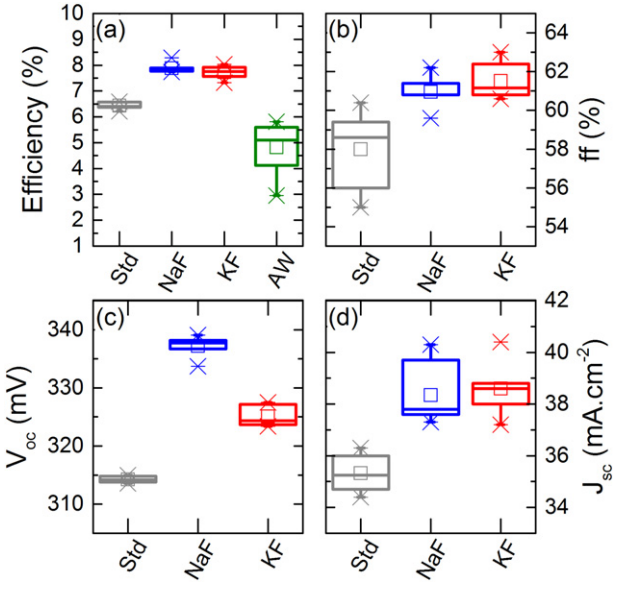

Fig. 2. (a)–(d): JV parameter distributions for solar cell sets made with untreated, NaF-treated and KF-treated absorbers and PDT without alkaline fluoride coating (Std, NaF, KF and AW respectively).

Please cite this article as: G. Rey et al., Post-deposition treatment of $Cu_2ZnSnSe_4$ with alkalis, Thin Solid Films (2016), http://dx.doi.org/10.1016/j.tsf.2016.11.021

and 3.7×10^{-6} mA·cm^{-2}, and a decrease in diode quality factor in average $A = 1.75$, 1.60 and 1.52 for Std, NaF and KF respectively. In addition, for KF-PDT an increase of the shunt resistance promotes the increase in V_{oc} (in average $R_{sh} = 147$, 141 and 169 Ω·cm^{-2} for Std, NaF and KF respectively).

Fig. 3 (a) shows the evolution of the V_{oc} with the temperature under 1 sun illumination. Within the one diode model, assuming that A and the reference current density are temperature independent and neglecting shunt conductance and voltage dependence of the carrier collection, the linear extrapolation of qV_{oc} (q being the elementary charge) to 0 K gives the activation energy of the main recombination path E_a^{mrp}. For the limiting case of bulk recombination, E_a^{mrp} is expected to equal E_g. However, for kesterite, due to potential or E_g fluctuations, E_a^{mrp} should be compared to the PL signal [26,32] which gives the energy of radiative bulk recombinations. The values of E_a^{mrp} of 844 meV, 849 meV and 858 meV for Std, NaF and KF samples, respectively, agree within measurement errors with the energy of the maximum of the PL spectra, plotted in Fig. 3 (b), found at 854 meV, 855 meV and 847 meV respectively, indicating that the main recombination occurs in the bulk. The value of $E_a^{mrp} =$ 858 meV measured for the KF sample is less accurate due to a slight variation of dV_{oc}/dT (bended curve). It is not possible to conclude on the increase in E_a^{mrp} seen after both post-deposition treatments as the variation is within measurement error. If confirmed such increase would have a positive effect on the V_{oc}.

Std and NaF samples show the same normalized PL spectrum. Because the PL at room temperature is mainly due to band-tail to band-tail recombination, the nature of the tail seems not to be changed by the Na-PDT, as could be expected from SIMS measurement since there is no incorporation of additional Na in the bulk of the film. The improved radiative efficiency (being the ratio between radiative recombination and radiative recombination plus non-radiative recombination and indicated by a higher PL intensity) seen after NaF-PDT could be attributed to a passivation effect of Na at the CdS/CZTSe interface or at the grain boundaries. The increase in radiative efficiency by factor of 1.2 seen after NaF-PDT cannot account entirely for the 28 mV difference in V_{oc} reported in Fig. 2 (c) since the change in quasi Fermi level splitting due to higher PL intensity is only $\Delta\mu \simeq k_B T \ln(1.2) \simeq 5$ meV. The red-shifted PL and the higher low-energy wing after KF-PDT suggests a higher density of tail or defect states possibly due to the incorporation of K in the bulk of the absorber. Despite this, KF-PDT has a beneficial effect on the radiative efficiency and thus on the V_{oc}. The red-shifted PL and the lower radiative efficiency of KF when compared to NaF explains why KF shows lower V_{oc} even though KF devices show improved j_0, A and R_{sh}.

From Fig. 3 (c) (showing the Tauc's plot derived from IQE data), since all linear extrapolations cross the energy axis at the same position, one can conclude that E_g was not modified by the PDT and therefore cannot account for the V_{oc} difference, E_a^{mrp} variations or PL shifts.

Capacitance spectra plotted in Fig. 4 show one main drop when decreasing the temperature and increasing the frequency which have been attributed to carrier or mobility freeze-out [26]. The capacitance spectra were fitted using Weiss method according to Ref. [33] and the extracted apparent defect densities are presented in Fig. 4. The higher activation energy of defects measured for the KF sample could possibly be due to a deeper acceptor level, that would increase the hole Fermi level in the band gap [16] thus limiting the V_{oc} improvement. These defects deeper in the band gap could also contribute to the higher defect density observed by PL. On the contrary, for NaF sample we observe shallower defects than in the Std sample; these shallower acceptors would help to further enhance the V_{oc}.

4. Conclusion

We applied low temperature (100 °C) post-deposition treatments with NaF and KF to CZTSe. KF-PDT increased the K concentration in the CZTSe film, whereas the change in Na could not be resolved by SIMS. The changes of Na concentration induced by NaF-PDT are small compared to the Na level already incorporated during the CZTSe growth as those changes might be limited to interfaces and grain boundaries. Both PDT lead to higher solar cell conversion efficiency driven by a simultaneous increase in *ff*, V_{oc} and J_{sc}. The V_{oc} improvement is attributed to a decrease in A and J_0 and to a better radiative efficiency. The best V_{oc} improvement was obtained with NaF-PDT which showed the highest radiative efficiency and the lowest activation energy of doping defects, whereas for KF-PDT the V_{oc} improvement was limited by red-shifted PL, larger band-tail state density and deeper acceptors. The highest J_{sc} was achieved with KF-PDT associated with larger space charge region width.

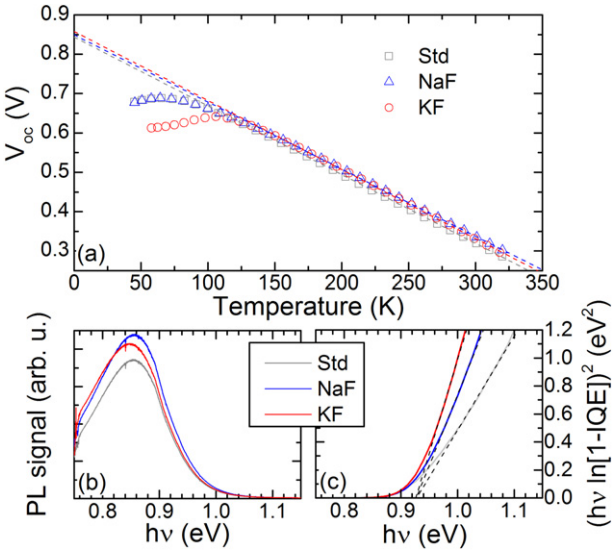

Fig. 3. (a): Temperature dependent V_{oc}. The linear fits show the extrapolation to 0 K for the determination of E_a^{mrp}. (b): PL spectra. (c): *IQE* derived Tauc's plots and band gap evaluation.

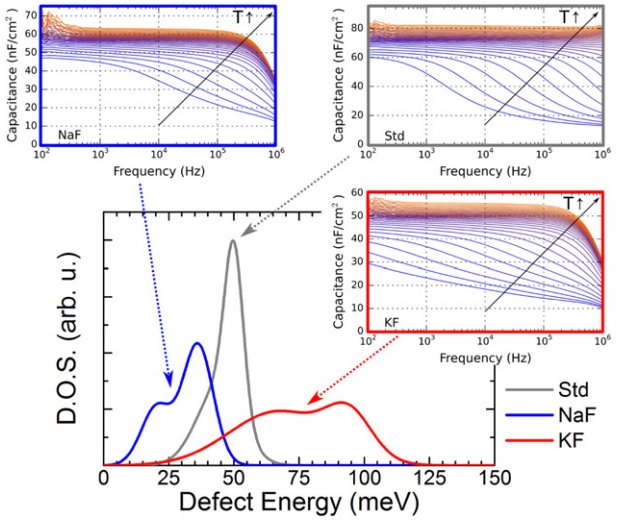

Fig. 4. Temperature dependent (from 45 K to 320 K) capacitance spectra.

Please cite this article as: G. Rey et al., Post-deposition treatment of $Cu_2ZnSnSe_4$ with alkalis, Thin Solid Films (2016), http://dx.doi.org/10.1016/j.tsf.2016.11.021

Acknowledgments

This work was funded by the Fonds National de la Recherche Luxembourg (FNR) under project KITS2 (C11/MS/1202439 – KITS2) and CURI-K (C14/MS/8267152/CURI-K). T. Schuler and P. Ramoa are acknowledged for their assistance.

References

[1] K. Ito, T. Nakazawa, Electrical and optical properties of stannite-type quaternary semiconductor thin films, Jpn. J. Appl. Phys. 27 (1988) 2094.
[2] L. Gütay, A. Redinger, R. Djemour, S. Siebentritt, Lone conduction band in $Cu_2ZnSnSe_4$, Appl. Phys. Lett. 100 (2012) 102113.
[3] N. Terada, S. Yoshimoto, K. Chochi, T. Fukuyama, M. Mitsunaga, H. Tampo, H. Shibata, K. Matsubara, S. Niki, N. Sakai, T. Katou, H. Sugimoto, Characterization of electronic structure of $Cu_2ZnSn(S_xSe_{1-x})4$ absorber layer and $CdS/Cu_2ZnSn(S_xSe_{1-x})4$ interfaces by in-situ photoemission and inverse photoemission spectroscopy, Thin Solid Films 582 (2014) 166–170.
[4] Y.S. Lee, T. Gershon, O. Gunawan, T.K. Todorov, T. Gokmen, Y. Virgus, S. Guha, $Cu_2ZnSnSe_4$ thin-film solar cells by thermal co-evaporation with 11.6% efficiency and improved minority carrier diffusion length, Adv. Energy Mater. 5 (2014) 1401372.
[5] G. Altamura, Développement de cellules solaires à base de films minces $Cu_2ZnSn(S,Se)_4$, Université de Grenoble. 2014. (Ph.D. thesis)
[6] O.W. Hlaing, J. Johnson, A. Bhatia, E. Lund, M. Nowell, M. Scarpulla, Grain size and texture of Cu_2ZnSnS_4 thin films synthesized by cosputtering binary sulfides and annealing: effects of processing conditions and sodium, J. Electron. Mater. 40 (2011) 2214–2221.
[7] T. Prabhakar, N. Jampana, Effect of sodium diffusion on the structural and electrical properties of Cu_2ZnSnS_4 thin films, Sol. Energy Mater. Sol. Cells 95 (2011) 1001–1004.
[8] S. Delbos, Këwhile thin films for photovoltaics: a review, EPJ Photovoltaics 3 (2012) 35004.
[9] T. Gershon, B. Shin, N. Bojarczuk, M. Hopstaken, D.B. Mitzi, S. Guha, The role of sodium as a surfactant and suppressor of non-radiative recombination at internal surfaces in Cu_2ZnSnS_4, Adv. Energy Mater. 5 (2015) 1400849.
[10] C.M. Sutter-Fella, J.A. Stückelberger, H. Hagendorfer, F.L. Mattina, L. Kranz, S. Nishiwaki, A.R. Uhl, Y.E. Romanyuk, A.N. Tiwari, Sodium assisted sintering of chalcogenides and its application to solution processed $Cu_2ZnSn(S,Se)_4$, Thin Film Solar Cells Chem. Mater. 26 (2014) 1420–1425.
[11] S. Lopez-Marino, Y. Sanchez, M. Espindola-Rodriguez, X. Alcobe, H. Xie, M. Neuschitzer, I. Becerril, S. Giraldo, M. Dimitrievska, M. Placidi, L. Fourdrinier, V. Izquierdo-Roca, A. Perez-Rodriguez, E. Saucedo, Alkali doping strategies for flexible and light-weight $Cu_2ZnSnSe_4$ solar cells, J. Mater. Chem. A 4 (2016) 1895–1907.
[12] O.P. Singh, K.S. Gour, R. Parmar, V.N. Singh, Sodium induced grain growth, defect passivation and enhancement in the photovoltaic properties of Cu_2ZnSnS_4 thin film solar cell, Mater. Chem. Phys. 177 (2016) 293–298.
[13] T. Schwarz, O. Cojocaru-Mirédin, P. Choi, M. Mousel, A. Redinger, S. Siebentritt, D. Raabe, Atom probe study of $Cu_2ZnSnSe_4$ thin-films prepared by co-evaporation and post-deposition annealing, Appl. Phys. Lett. 102 (2013) 042101.
[14] S. Tajima, R. Asahi, D. Isheim, D.N. Seidman, T. Itoh, K. ichiro Ohishi, Sodium distribution in solar-grade Cu_2ZnSnS_4 layers using atom-probe tomographic technique, Jpn. J. Appl. Phys. 54 (2015) 112302.
[15] L.Q. Phuong, M. Okano, G. Yamashita, M. Nagai, M. Ashida, A. Nagaoka, K. Yoshino, Y. Kanemitsu, Photocarrier dynamics in undoped and Na–doped Cu_2ZnSnS_4 single crystals revealed by ultrafast time-resolved terahertz spectroscopy, Appl. Phys. Express 8 (2015) 062303.
[16] J.V. Li, D. Kuciauskas, M.R. Young, I.L. Repins, Effects of sodium incorporation in co-evaporated $Cu_2ZnSnSe_4$ thin-film solar cells, Appl. Phys. Lett. 102 (2013) 163905.
[17] A. Nagaoka, H. Miyake, T. Taniyama, K. Kakimoto, Y. Nose, M.A. Scarpulla, K. Yoshino, Effects of sodium on electrical properties in Cu_2ZnSnS_4 single crystal, Appl. Phys. Lett. 104 (2014) 152101.
[18] Y.-R. Lin, V. Tunuguntla, S.-Y. Wei, W.-C. Chen, D. Wong, C.-H. Lai, L.-K. Liu, L.-C. Chen, K.-H. Chen, Bifacial sodium-incorporated treatments: tailoring deep traps and enhancing carrier transport properties in Cu_2ZnSnS_4 solar cells, Nano Energy 16 (2015) 438–445.
[19] B.T. Gershon, Y.S. Lee, R. Mankad, O. Gunawan, T. Gokmen, D. Bishop, B. McCandless, S. Guha, The impact of sodium on the sub-bandgap states in CZTSe and CZTS, Appl. Phys. Lett. 106 (2015) 123905.
[20] M. Bär, B.-A. Schubert, B. Marsen, S. Krause, S. Pookpanratana, T. Unold, L. Weinhardt, C. Heske, H.-W. Schock, Native oxidation and Cu-poor surface structure of thin film Cu_2ZnSnS_4 solar cell absorbers, Appl. Phys. Lett. 99 (2011) 112103.
[21] H. Xie, S. López-Marino, T. Olar, Y. Sánchez, M. Neuschitzer, F. Oliva, S. Giraldo, V. Izquierdo-Roca, I. Lauermann, A. Pérez-Rodríguez, E. Saucedo, Impact of Na dynamics at the $Cu_2ZnSn(S,Se)_4$/CdS interface during post low temperature treatment of absorbers, ACS Applied Materials & Interfaces 8 (2016) 5017–5024.
[22] Z. Tong, C. Yan, Z. Su, F. Zeng, J. Yang, Y. Li, L. Jiang, Y. Lai, F. Liu, Effects of potassium doping on solution processed kesterite Cu_2ZnSnS_4 thin film solar cells, Appl. Phys. Lett. 105 (2014) 223903.
[23] E. Ghorbani, J. Kiss, H. Mirhosseini, T.D. Kühne, C. Felser, Hybrid functional calculations on the Na and K impurities in substitutional and interstitial positions in $Cu_2ZnSnSe_4$, Photovoltaic Specialist Conference (PVSC), 2015 IEEE 42nd, New Orleans, LA, 2015, pp. 1–3. http://dx.doi.org/10.1109/PVSC.2015.7356099.
[24] W. Xiao, J. Wang, X. Zhao, J. Wang, G. Huang, L. Cheng, L. Jiang, L. Wang, Intrinsic defects and Na doping in Cu_2ZnSnS_4: a density-functional theory study, Sol. Energy 116 (2015) 125–132.
[25] T. Maeda, A. Kawabata, T. Wada, First-principles study on alkali-metal effect of Li, Na, and K in Cu_2ZnSnS_4 and $Cu_2ZnSnSe_4$, Phys. Status Solidi C 12 (2015) 631–637.
[26] G. Rey, T. Weiss, J. Sendler, A. Finger, C. Spindler, F. Werner, M. Melchiorre, M. Hála, M. Guennou, S. Siebentritt, Ordering kesterite improves solar cells: a low temperature post-deposition annealing study, Sol. Energy Mater. Sol. Cells 151 (2016) 131–138.
[27] A. Redinger, J. Sendler, R. Djemour, T. Weiss, G. Rey, P. Dale, S. Siebentritt, Different bandgaps in $Cu_2ZnSnSe_4$: a high temperature coevaporation study, Photovoltaics IEEE J. 5 (2015) 641–648.
[28] M.A. Contreras, M.J. Romero, B. To, F. Hasoon, R. Noufi, S. Ward, K. Ramanathan, Optimization of CBD CdS process in high-efficiency $Cu(In,Ga)Se_2$-based solar cells, Thin Solid Films 403–404 (2002) 204–211.
[29] M. Hála, S. Fujii, A. Redinger, Y. Inoue, G. Rey, M. Thevenin, V. Deprédurand, T.P. Weiss, T. Bertram, S. Siebentritt, Highly conductive ZnO films with high near infrared transparency, Prog. Photovolt. Res. Appl. 23 (2015) 1630–1641.
[30] T.P. Weiss, A. Redinger, G. Rey, T. Schwarz, M. Spies, O. Cojocura-Mirdin, P.-P. Choi, S. Siebentritt, Impact of annealing on electrical properties of $Cu_2ZnSnSe_4$ absorber layers, J. Appl. Phys. 120 (2016) 045703.
[31] S.S. Hegedus, W.N. Shafarman, Thin-film solar cells: device measurements and analysis, Prog. Photovolt. Res. Appl. 12 (2004) 155–176.
[32] S. Siebentritt, G. Rey, A. Finger, J. Sendler, T. Weiss, D. Regesch, T. Bertram, What is the bandgap of kesterite? Sol. Energy Mater. Sol. Cells 158 (2016) 126–129.
[33] T. Weiss, A. Redinger, D. Regesch, M. Mousel, S. Siebentritt, Direct evaluation of defect distributions from admittance spectroscopy, IEEE J. Photovoltaics 4 (2014) 1665–1670.

Please cite this article as: G. Rey et al., Post-deposition treatment of $Cu_2ZnSnSe_4$ with alkalis, Thin Solid Films (2016), http://dx.doi.org/10.1016/j.tsf.2016.11.021